Long-term tectonothermal history of Laramide basement from zircon-He age-eU correlations

Devon A. Orme[1], William R. Guenthner[2], Andrew K. Laskowski[3] and Peter W. Reiners[3]

[1]Department of Geological Sciences, Stanford University, Stanford, California, USA
[2]Department of Geology, University of Illinois, Urbana-Champaign, Champaign, Illinois, USA
[3]Department of Geosciences, University of Arizona, Tucson, Arizona, USA

Corresponding author: D.A. Orme, dorme@stanford.edu

Abstract

The long-term (> 1 Ga) thermal histories of cratons are enigmatic, with geologic data providing only limited snapshots of their evolution. We use zircon (U-Th)/He (zircon He) thermochronology and age-composition correlations to understand the Proterozoic-Phanerozoic thermal history of Archean Wyoming province rocks exposed in the northern Laramide ranges of western North America. Zircon He ages from the Wind River Range (54 dates) and Bighorn Mountains (32 dates) show negative correlations with effective uranium (eU), a proxy for radiation damage. Zircon dates from the Bighorns are between 960 Ma (low-eU) and 20 Ma (high-eU) whereas samples from the Wind Rivers are between 582 Ma (low-eU) and 33 Ma (high-eU). We applied forward modeling using the zircon radiation damage and annealing model ZrDAAM to understand this highly variable dataset. A long-term *t-T* path that is consistent with the available geologic constraints successfully reproduced age-eU correlations. The best fit to the Wind Rivers data involves two phases of rapid cooling at 1800-1600 Ma and 900-700 Ma followed by slower cooling until 525 Ma. During the Phanerozoic, these samples were heated to maximum temperatures between 160-125°C prior to Laramide cooling to 50ºC between 60-40 Ma. Data from the Bighorn Mountains were successfully reproduced with a similar thermal history involving cooler Phanerozoic temperatures of ~115 °C and earlier Laramide cooling between 85-60 Ma. Our results indicate that age-eU correlations in zircon He datasets can be applied to extract long-term thermal histories that extend beyond the most recent cooling event. In addition, our results constrain the timing, magnitude and rates of cooling experienced by Archean Wyoming Province rocks between recognized deformation events, including the >1 Ga period represented by the regionally-extensive Great Unconformity.

1. Introduction

Basement rocks of the Laramide ranges of northwestern Wyoming experienced a protracted thermal history involving multiple burial and exhumation episodes since their formation during the Archean. Geologic and geochronologic data indicate that prior to

44 their most recent exhumation in the Cenozoic and burial by several kilometers of
45 sediment in the Paleozoic and Mesozoic, these rocks were affected by multiple
46 Proterozoic tectonic events such as supercontinent assembly and rifting (e.g.,
47 Chamberlain et al. 2003; Marshak et al., 2000). However, specific constraints on the
48 time-Temperature (*t*-*T*) history of the region remain enigmatic. Understanding the early
49 Proterozoic-Mesozoic thermal history enables an integrated long-term history that could
50 reveal previously undocumented events, including thermal maturation, cratonal stability,
51 and orogenesis. Apatite fission track (AFT) and (U-Th)/He (apatite He)
52 thermochronology has previously been used to resolve the thermal histories of cratons,
53 typically over 10^8-year time scales (e.g., Gleadow et al., 2002; Kohn et al., 2005;
54 Flowers, 2009; Ault et al. 2009; 2013). The broad temperature sensitivity of the zircon
55 (U-Th)/He (zircon He) system enables recovery of even longer, billion-year thermal
56 histories. This study utilizes recent advances in our understanding of the influence of
57 radiation-damage on He diffusion in zircon (Guenthner et al., 2013; Guenthner et al.
58 2014) to elucidate major features of a ~2 Ga thermal history of Laurentian basement
59 rocks in western North America.
60 Zircon He dating can be combined with radiation damage and annealing modeling
61 to recover long-term thermal histories when varying amounts of radiation damage
62 accumulate over time in grains with different U-Th concentrations from the same sample
63 (Powell et al. 2016; Guenthner et al. 2015). These variations produce a range of He
64 diffusivities and closure temperatures (T_c) such that each grain records a different He age.
65 Among grains that experience the same thermal history, differences are proportional to
66 differences in effective uranium (eU, U + 0.235 x Th). Correlations between He age and

67 eU therefore reflect the coevolution of the sample's thermal history and radiation damage
68 and damage annealing of its zircon grains. More specifically, the retentivity of He in
69 zircon, and therefore the T_c, initially increases with progressive damage accumulation to
70 a critical threshold after which retentivity and T_c decrease (Guenthner et al., 2013;
71 Guenthner et al. 2014). Given the initial increase and subsequent decrease in T_c, the
72 damage-diffusivity relationship typically manifests as positive (increasing T_c with
73 increasing eU) or negative correlations (decreasing T_c with increasing eU) between single
74 grain ages and their eU concentrations.
75 In this paper, we present the first zircon He ages from the Wind River Range,
76 which were obtained from a suite of samples collected and analyzed for AFT by Cerveny
77 and Steidtmann (1993). We also present new zircon He data from the Bighorn Range
78 (Fig. 1). Zircon grains from samples in both regions show strong negative age-eU
79 correlations, which we use in combination with the radiation damage-based model for He
80 diffusion in zircon (ZRDAAM) from Guenthner et al. (2013) to resolve distinct *t*-*T*
81 relationships. Our new *t*-*T* constraints describe not only the most recent phase of
82 exhumation related to Laramide orogenesis, but previous cooling and heating episodes
83 spanning ~2 Ga. In geologic settings where evidence of previous thermal events is
84 overprinted or eroded, low-temperature thermochronology has the ability to reconstruct
85 its long-term thermal history.
86
87 **2. Geologic Setting**
88 The ~6000 km^2, northwest-southeast trending Wind River Range and the ~4500
89 km^2, north-south trending Bighorn Mountains of Wyoming are two of the most

prominent features in the Laramide Province, which comprises mountain ranges bound by high-angle reverse faults that cut crystalline basement rocks (Fig. 1). The cores of the these ranges consist of Archean granite, granitic gneiss, and granodiorite of the Wyoming Province that amalgamated with other Archean cratons to form Laurentia during the Paleoproterozoic (2.0-1.8 Ga) Trans-Hudson orogeny (Hoffman, 1988). Between 1.8-1.7 Ga, juvenile crust accreted to the southeastern margin of Laurentia along the Cheyenne belt of southeastern Wyoming as part of the Yavapai and Mazatzal orogenies (Houston, 1993; Chamberlain, 1998; Whitmeyer and Karlstrom, 2007). Sometime between ~1.7-0.5 Ga, Archean rocks in the core of the Wind River Range and Bighorn Mountains were exhumed to the surface. Later, these rocks were buried under 4-6 km of Paleozoic and Mesozoic passive margin strata. Finally, they were exhumed in the cores of Laramide ranges in the hanging walls of high-angle reverse faults related to Cenozoic orogenesis.

In western North America, the contact between Archean igneous and metamorphic rocks and overlying Paleozoic strata is referred to as the "Great Unconformity". The ~2 Ga of missing geologic record across this contact represents nearly half of Earth's history and as such, the thermal and tectonic history is largely unconstrained during this interval. Previous low-temperature thermochronology datasets (apatite He and AFT) were completely reset by the youngest cooling episode, related to slip across Laramide reverse faults. However, high-temperature thermochronology studies have shown limited evidence of prior cooling, including biotite K-Ar ages of ~ 2.0-1.5 Ga in the Wind River Range (Peterman, 1979). In the Bighorn Mountains, biotite K-Ar ages indicate > 2.5 Ga cooling (Heimlich and Armstrong, 1972).

Regional geologic field investigations data indicate that two phases of extension affected the interior of the Wyoming craton, between 1300-1000 Ma and 900-700 Ma (Chamberlain et al. 2003; Mueller and Frost, 2006). The timing and orientation of extensional structures suggest they are far-field effects of the ~1.2-1.0 Ga Grenville collisional orogen and/or Neoproterozoic-early Paleozoic Iapetan rifting (Timmons et al., 2000). The latter event is evidenced by retrograde metamorphism along Precambrian deformation zones dated at ~900 Ma in the Wind River Range (Mitra and Frost, 1981). Various authors interpret that inherited crustal weak zones related to extensional structures controlled the orientation of Cenozoic reverse faults that bound the Laramide ranges (e.g. Marshak and Paulsen, 1996; Marshak et al. 2000; Timmons et al. 2001), suggesting that these events affected Archean rocks in the Wind River Range and Bighorn Mountains.

3. Previous Low-Temperature Thermochronologic Results

Low-temperature thermochronology of Archean basement is restricted to apatite He and AFT studies sensitive only to the most recent Cenozoic or "Laramide-age" phase of exhumation (Shuster, 1986; Steidtmann et al., 1989; Cerveny, 1990; Crowley et al. 2002; Peyton et al. 2012). Cerveny and Steidtmann (1993) obtained AFT ages from crystalline basement from the Wind River Range, which they interpreted as requiring exhumation through depths of ~4 km as early as 85 Ma, followed by two periods of rapid cooling between 62-57 Ma and 40 Ma. More recent work by Peyton et al. (2012) and Stevens et al. (2016) found AFT ages of 57-54 Ma and 61-42 Ma in samples collected near Gannett, Temple, and Fremont Peaks, respectively. Thermal modeling of track-

length distributions and ages by Stevens et al. (2016) were interpreted to require rapid cooling at ~65-50 Ma. These authors modeled maximum burial temperatures in the 135 to 160 °C range just prior to Laramide cooling.

Apatite He ages from the crystalline core of the Bighorn Mountains are 369-60 Ma, and were interpreted to record a pre-Laramide He partial retention zone (PRZ) exhumed around ~65-70 Ma (Reiners and Farley, 2001; Crowley et al., 2002; Peyton et al., 2012). Subsurface samples from a ~4.5-km deep borehole on the east side of the range are predominantly 60-70 Ma near the surface and as young as 3 Ma at depths about 5 km beneath the Great Unconformity (Peyton et al., 2012). Reiners and Farley (2001) used age-grain-size correlations to infer pre-Laramide burial temperature of ~65-80 °C. Merging a larger data set with previous surface and borehole results, Peyton et al. (2012) found best-fit models for about 50 °C of Laramide cooling beginning by 85 Ma and ending at ~60 Ma. Peyton et al.'s (2012) inverse modeling suggested maximum pre-Laramide temperatures ranging from ~80 to ~115 ºC for certain *t-T* paths but did not consider *t-T* paths that began before 200 Ma, which may be important for radiation damage effects (e.g., Shuster et al., 2006; Flowers et al., 2009; Gautheron et al., 2009). We use the approximate timing (~85-60 Ma) and maximum temperature (~80-120 °C) of Laramide exhumation in the Bighorns as a guideline for our interpretations.

4. Zircon He Results

We dated 54 single-crystal aliquots of zircon from 9 samples along the range-perpendicular Middle Fork Transect in the Wind River Range (2567-3534 m above sea level) from the original mineral separates acquired by Cerveny and Steidtmann (1993) (Fig. 1). We followed methods described in Reiners et al. (2004) (Appendix I). Zircon He

ages range from 581±8.1 to 33.2±0.45 Ma and show no correlation with grain size, or, with the exception of WY-100-89 and WY-101-89, elevation (Fig. 2A; Appendix I; Supplementary Material I). However, zircon He ages correlate strongly with eU (Fig. 2A), over an eU range of 270-7200 ppm. The correlation with age is strongly negative at eU values less than ~850 ppm, but younger ages form a long tail of relatively restricted ages between 61-33 Ma across a wide range of higher eU (i.e. 850-7200 ppm).

We dated 32 single zircon crystals from the northeastern part of the Bighorn Mountains at Bald Mountain (Samples BaldMtn-1-12 and 5SP-1-12; 2397-2824 m), along Shell Canyon (Samples BH12, BH17, and SC-2-12; 1808-2410 m), and at Burgess Junction (BJ-1-12). Single grain ages range from 956±14.7 to 6.10±0.09 Ma (Fig. 2B) and do not correlate with grain size or elevation. These samples show a similar inverse age-eU correlation as the Wind River samples, but across a lower range of eU, (~200-1000 ppm). These results are similar to those from the BH12 and BH17 samples of Guenthner et al. (2013) (Fig. 2B).

5. Thermal-History Modeling

Thermal-history (*t*-*T*) modeling can be used to assess the validity of potential *t*-*T* paths (hypotheses) for producing a set of thermochronometric ages. We used this approach to investigate whether our data are compatible with expectations of the geologic history of the region and to constrain specific *t*-*T* segments of our sample thermal histories that were not resolved by apatite He and AFT data presented in previous studies (i.e. the Proterozoic thermal history). We used a forward modeling approach to constrain possible *t*-*T* paths, using a portion of the relevant code from the program HeFTy (i.e., He diffusion modeling with alpha ejection correction and ZrDAAM; Guenthner et al., 2013)

183 implemented in Matlab in order to handle a large number of single grain inputs and more
184 easily output model age-eU correlations. This code was checked against HeFTy outputs
185 to confirm similarities.
186 We favored a forward modeling approach as inverse modeling requires averaging
187 of grain-specific inputs (i.e. grain size, U and Th concentrations) and typically only
188 displays modeled date-eU correlations for the best-fit *t-T* paths. This in turn makes it
189 difficult to visually a specific *t-T* path date-eU correlation. Visual inspection is important
190 when dealing with apatite and zircon He data, as the statistical tests employed in inverse
191 models critically assume that all sources of date variation are well constrained. In reality,
192 some sources of date variation are better accounted for (e.g. grain size, radiation damage
193 effects) than others (e.g. U and Th zonation). For these reasons, the forward approach
194 better demonstrates the extent to which date variation in zircon He datasets can be
195 explained by ZRDAAM and is thus better suited for our purposes.
196 For modeling purposes, we combined single grain aliquots from individual
197 samples into either a single suite of ages (Bighorn dataset) or distinct groups (Wind River
198 dataset). The Bighorn ages can be interpreted as a single group because: 1) all ages from
199 a given suite form a single, coherent negative age-eU correlation, suggesting that
200 radiation damage is the primary source of intra- and intersample age variation, and 2) all
201 samples were collected within the same approximate depth relative to the Great
202 Unconformity (and are not separated by major faults), which suggests that samples in a
203 given dataset share a common thermal history. The Wind River dataset is complicated by
204 the lack of a single coherent negative trend and differences in sample elevation. In figure
205 2A, a distinct group of ages from samples WY-96-89 and WY-98-89 has a range of 200-

206 600 Ma with eU concentrations between ~200 and 300 ppm. This group appears shifted
207 towards lower eU concentrations at a given age relative to the rest of the main negative
208 trend, and should therefore be modeled with a separate thermal history. This observation
209 is strengthened by the age-elevation relationship for the full Wind River dataset
210 (Supplementary Material, Fig. 1). Although no clear correlation between age and
211 elevation is apparent for the majority of the dataset, we note that WY-98-89 and WY-96-
212 89 are two of the lowest elevation samples, positioned closest to the main Wind River
213 thrust (Fig. 1), suggesting that they are more deeply exhumed than the higher elevation
214 samples. Age-elevation relationships also show that samples WY-100-89 and WY-101-
215 89 lie below the Laramide paleo-PRZ and were likely fully reset. Indeed, these samples
216 display nearly flat correlations between age and eU. For modeling purposes, we therefore
217 consider WY-98-89 and WY-96-89 as a separate group and exclude WY-100-89 and
218 WY-101-89.
219 To interpret age-eU correlations, ZRDAAM combines the damage-diffusivity
220 relationship (Guenthner et al., 2013) with a damage-annealing model defined by a
221 fanning curvilinear fit to the zircon fission track (ZFT) annealing data of Yamada et al.
222 (2007). Annealing kinetics give a ZFT partial annealing zone (PAZ) of 310-223 ºC (0.4-
223 0.8 mean length reduction ratio, 10 Ma isothermal hold-time). These kinetics are
224 currently the best available option for describing how the radiation damage that affects
225 He diffusivity anneals over geologic timescales. Although more work is needed to better
226 define damage annealing in zircon, the primary relationships between accumulated
227 damage and He diffusivity provide strong constraints on the thermal histories under the

228 reasonable assumption (considering sedimentary and tectonic reconstructions) that little
229 to no damage annealing occurred after Neoproterozoic.

230 **5.1 Model inputs**

231 Our model takes grain size, U and Th concentrations, and *t*-*T* paths as inputs
232 (Appendix II). For grain size, we model three separate age-eU curves for each *t*-*T* path
233 using the mean grain size ± two standard deviations for each dataset. The resulting output
234 is an envelope with a central curve that shows the extent to which the combined effects of
235 grain size and radiation damage explain the observed age variation.

236 In choosing our input *t*-*T* paths, we considered the geologic observations and
237 previously published thermochronometric results described in previous sections. Few
238 constraints on the geologic history of these rocks are available between their formation in
239 the Archean and deposition of basal Cambrian strata (i.e. the Great Unconformity). As
240 discussed above, a few K-Ar ages from the southernmost Wind Rivers hint at cooling
241 below ~300 °C at approximately 1500 Ma. The next nearest constraints are Rb/Sr data
242 from the Laramie Range in southeastern Wyoming, which suggest an ~1.78 Ga
243 metamorphic cooling event (Patel et al., 1999). Similarly, K-Ar hornblende and U-Pb
244 apatite ages within the Laramie Peak shear zone and Cheyenne Belt are interpreted to
245 record rapid uplift during Cheyenne belt deformation between 1.8-1.6 Ga (Chamberlain
246 et al., 1993). However, no thermochronologic data are available that describe the
247 subsequent 1.2 b.y. of geologic history. As such, our *t*-*T* inputs are primarily designed to
248 examine when major Proterozoic cooling (exhumation) initiated in each range, how much
249 cooling occurred, and how long-lived the Proterozoic cooling episode was. We have also
250 designed our specific paths to be consistent with previously published constraints for the

timing of Laramide exhumation, although this is not our main focus. For the Wind River Range, we use the approximate timing of 60—40 Ma, in agreement with the constraints discussed above. Fan and Carrapa (2014) modeled Laramide-related cooling to ~50 °C, and we used this as the temperature at the end of Laramide cooling. For the Bighorn Mountains, we again used the inverse model results from Peyton et al. (2012) to define the timing of Laramide-related exhumation—85 to 60 Ma—as well as the temperatures at the end of Laramide exhumation event—50 °C. We considered the maximum Phanerozoic burial temperatures achieved just prior to Laramide cooling as a variable and a more detailed investigation of these temperatures for both datasets is discussed in subsequent sections.

Our forward modeling follows an iterative process in which we continually narrow our search of Proterozoic *t-T* space, and the discussion of specific *t-T* tests and model results in this section reflects that approach. We first model "end-member" thermal histories, followed by "representative" and then "refined" thermal histories. With each subsequent iteration, our objective was to bracket the observed data to arrive at the most acceptable solution. Model *t-T* paths are as parsimonious as possible given principal geologic constraints outlined above, and, given the lack of constraints on the Proterozoic thermal history of our samples, this simplifying approach does not over interpret the data or lead overly complex and unwarranted models. Additional complexities, such as considering the precise burial history from unit thickness-age variations in the stratigraphic record, would likely have only a minor effect on the model age-eU correlations (e.g. Guenthner et al., 2015).

274 **5.2 End member scenario and results**

275 Our most extreme end-member *t-T* path forward models (Fig. 3A) are focused on
276 distinguishing whether earliest or latest Proterozoic cooling can reproduce the basic
277 features of the age-eU correlation. The two end-member thermal histories assume rapid
278 cooling from well above zircon He PRZ temperatures from either 2600 to 2500 Ma
279 (corresponding to the approximate age of high-grade, granulite-facies metamorphism in
280 both ranges (Frost and Frost, 1993)), and or from 700 Ma to the mid-Cambrian,
281 simulating Neoproterozoic formation of the Great Unconformity. The Phanerozoic
282 portion of the thermal history that involves relatively well-constrained burial and
283 Laramide exhumation is kept constant in this set of models; details of this portion of the
284 path have little effect on the results. In both cases, cooling starts at 350 °C to allow our
285 samples to cool fully through the ZFT partial annealing zone (PAZ) and ends at surface
286 temperatures of 20 °C (Fig. 3A). These end-member scenarios represent roughly the
287 maximum and minimum amount of time that our datasets could have spent at near-
288 surface temperatures in the Proterozoic.

289 The Phanerozoic portions for these and all subsequent "representative" paths
290 begin with the middle Cambrian (525 Ma) deposition of the Flathead Sandstone,
291 followed by the Laramide constraints described above with reheating to 160 °C for the
292 Wind River dataset and 120 °C for the Bighorn dataset. We chose 120 and 160 °C in part
293 because these are the maximum burial temperatures modeled by Peyton et al. (2012) and
294 Fan and Carrapa (2014), respectively, but they also simulate intermediate temperatures
295 while keeping the model grains below the conventional zircon He T_c of ~180 °C. Models
296 with these temperatures closer to 180 °C lead to nearly flat age-eU curves as all of the

297 grains are reset to ages much younger than those observed in either dataset at both low
298 and high eU concentrations. For these initial tests, we did not attempt to refine the late-
299 stage portions of the thermal history most relevant to Laramide exhumation, but expand
300 upon these particular inputs in our "refined" thermal history models.

301 Model outputs for the two end-member *t-T* paths are shown in figure 3B. In both
302 datasets, the model age-eU correlations cross-over and bracket the observed age-eU
303 trends. Rapid Paleoproterozoic cooling (path 1 in fig. 3A) produces model correlations at
304 much lower eU values than the observations, whereas much younger Neoproterozoic
305 cooling leads to ages that are far too young at low eU to explain the Bighorn age-eU
306 trends, or too old at intermediate eU to explain the Wind River trends. These results
307 indicate that major cooling events in either the earliest or latest Proterozoic do not satisfy
308 the observations but their crossover bracketing of the data suggest an intermediate
309 solution may be a better solution.

310 **5.3 Representative scenarios and results**

311 With the end member results in mind, we constructed a series of different
312 representative paths that further tested the Proterozoic *t-T* space, while exploring the
313 specific hypotheses of Proterozoic tectonism previously discussed. These geologic events
314 include: 1) the 1800-1600 Ma Yavapai-Mazatazal orogenic event as expressed in the
315 crustal suturing along the Cheyenne Belt of southeastern Wyoming (Houston, 1993;
316 Chamberlain, 1998), 2) two episodes of rifting related extension at 1300-1000 Ma and
317 900-700 Ma (Marshak et al., 2000; Timmons et al., 2001), and 3) Neoproterozoic erosion
318 (~700 Ma to 542 Ma) associated with the creation of the Great Unconformity.

In figures 4A and 5A we show *t-T* paths that represent these proposed events and consist of either initial rapid cooling to surficial temperatures over a given time (Fig. 4A), or a two-stage monotonic cooling with prolonged residence at intermediate temperatures (Fig. 5A). We also considered a *t-T* path with linear cooling beginning at 1800 Ma (Fig. 5A) as described below. For the Proterozoic intermediate temperatures, we initially chose 170 °C because it simulates long term residence at the low temperature boundary of the conventional PRZ and therefore would not fully reset ages during the Proterozoic. Higher intermediate temperatures from 1600 Ma to 900 Ma, for example, would more fully reset zircon He ages and in effect produce model age-eU curves similar to rapid cooling at 900 Ma, which partially defeats the purpose of exploring representative thermal histories. We further tested this intermediate temperature with our refined thermal histories.

The results from these representative *t-T* paths are compared to the observed Wind River and Bighorn datasets (Fig. 4B and 5B). In all three rapid cooling scenarios for the Bighorn data (Figs. 4Bi, 4Biii, and 4Bv), the model curves are too young at most eU concentrations. Furthermore, no combination of model curves brackets the observed ages, which suggests that a *t-T* path with rapid cooling from high temperature to near surface temperatures in the Proterozoic is not a viable solution. In contrast, for the Wind River data, scenarios 1 (1800-1600 Ma cooling, Fig. 4Bii) and 3 (900-700 Ma cooling, Fig. 4Bvi) yield model curves that bracket almost all of the observed ages, with scenario 3 capturing 33 of the 43 single grain ages (77%). The "intermediate" scenario 2 (1300-1000 Ma rapid cooling, Fig. 4Biv) appears to split the other two scenarios and also reproduces 77% of the observed ages. Importantly though, both scenarios 2 and 3 miss the distinctive cluster of young ages at low eU, and model age-eU curves remain too old

342 for this cluster even with further modification of maximum Phanerozoic temperatures
343 (see next section for more details). For these reasons, we do not consider *t-T* paths for
344 either the Bighorns or Wind Rivers from figure 4 in our refined scenarios.
345 Our two-stage or linear cooling paths (Fig. 5) help to refine our search for viable
346 *t-T* hypotheses. For the Bighorns dataset, only thermal scenario 2 (two stages of major
347 cooling at 1800-1600 Ma and 900-525 Ma) replicates a high number of observed ages, as
348 well as the overall form of the observed age-eU correlation (age plateau at low eU,
349 steeply negative correlation, age pediment at high eU) (Fig. 5Biii). All other scenarios
350 give ages that are too young at most eU concentrations. Results are more ambiguous for
351 the Wind River dataset. All three two-stage models give roughly the same model curves:
352 they reproduce the group of ~200-600 Ma grains at approximately 150-300 ppm eU, but
353 are too young at a given eU concentration for the majority of the ages (Figs. 5Bii, 5Biv,
354 and 5Bvi). A *t-T* path with linear cooling from 1800 to 525 Ma (scenario 4) appears to
355 yield model curves that shift slightly towards older ages, but still captures relatively few
356 ages (19 out of 43, Fig. 5Bviii).
357 Altering the intermediate Proterozoic and maximum Phanerozoic temperatures in
358 these Wind River scenarios (Figs. 5Bii, 5Biv, and 5Bvi) could result in model curves that
359 encompass more ages. We consider *t-T* paths that both increase and decrease these
360 temperatures. Because the Wind River models tend to give ages that are too young at
361 most eU concentrations, none of these three model outputs are significantly changed by
362 increasing the Phanerozoic maximum burial temperature. That is, higher maximum burial
363 temperatures cause flatter age-eU correlations and a further shift towards younger ages
364 and the fit to the observed data is not improved. Decreasing these temperatures, however,

365 produces model curves with a broader age range and older results that could better model
366 the observed data. Decreasing the maximum Phanerozoic burial temperatures also
367 provides some leverage on achieving better model results. These segments of the *t*-*T* path
368 are partially constrained by the previous apatite He and AFT modeling efforts, but the
369 previous thermal models give a range of burial temperatures, and it is important to
370 consider this entire range.

371 **5.4 Refined scenarios and results**

372 Our refined tests explored one representative *t*-*T* path for the Bighorn dataset
373 (scenario 2 in Fig. 5Biii) and three representative *t*-*T* paths for the Wind River (scenarios
374 1, 2, and 3 in Fig. 5Bii, 5Biv, and 5Bvi). These tests involved varying the two remaining
375 parameters that are least well known: the intermediate temperature to which rocks
376 initially cooled in the Proterozoic, and the maximum temperature to which rocks were
377 reheated by pre-Laramide burial. For the former we examined *t*-*T* paths across a wide
378 range of intermediate Proterozoic temperatures (100 °C to 300 °C) in increments of 5 °C.
379 For the latter, in the Bighorns, we tested the previously modeled range of Phanerozoic
380 maximum temperatures between 80 and 120 °C (Peyton et al., 2012), and in the Wind
381 Rivers, we tested between 120 and 160 °C (Fan and Carrapa, 2014).

382 Two model scenarios for the refined Bighorn thermal histories are shown in figure
383 6. The first (scenario 1) consists of a Proterozoic intermediate temperature of 155 °C and
384 a Phanerozoic maximum burial temperature of 110 °C. A slightly higher intermediate
385 temperature of 160 °C and burial temperature of 110 °C yield the model ages shown in
386 scenario 2 from this figure. Intermediate temperatures less than ~145 °C and greater than
387 ~180 °C shift the low eU portions of the model curve to older and younger ages,

388 respectively, and miss the observed ages at lowest eU. In all scenarios that we tested, the
389 cluster of 20-40 Ma ages at high eU was never fully encompassed by the 2-sigma
390 envelope, but some tested *t-T* paths do capture the average trend of this cluster. We
391 emphasize, however, that regardless of the precise intermediate Proterozoic or maximum
392 Phanerozoic temperatures, the data appear to require two major phases of Precambrian
393 cooling, one in the Paleoproterozoic (1800-1600 Ma) and a later one to near-surface
394 temperatures in the Neoproterozoic (900-525 Ma).
395 The refined thermal history models for the Wind River dataset do not produce a
396 single preferred solution for all samples. Instead, we considered the Wind River data as
397 comprising two groups of samples with slightly different thermal histories. This is
398 consistent with the two sample groups being collected at different elevations with one
399 group at lower elevations (samples WY-98-89 and WY-96-89) likely experiencing higher
400 maximum temperatures. To reflect differences in elevation, we constrained the two
401 refined best-fit *t-T* paths to have the same general form with two stages of cooling, one at
402 1800-1600, and another at either 1300-1100, 900-525, or 700-525 Ma (Figs. 5Bii, 5Biv,
403 and 5Bvi), but slightly different maximum Phanerozoic temperatures and different
404 intermediate temperatures between the two Proterozoic stages of cooling. These *t-T* tests
405 therefore consisted of a matrix of 320 individual *t-T* paths (see above, 100 to 300 °C for
406 Proterozoic intermediate, and 120 to 160 °C for Phanerozoic maximum temperatures,
407 both tested in increments of 5 °C) applied to each two-stage cooling scenario (Figs. 5Bii,
408 5Biv, and 5Bvi) and each distinct sample group.
409 Following this approach, a range of refined *t-T* paths provides the best results for
410 either distinct sample group (Fig. 7A). Specific *t-T* paths within the temperature ranges

411 discussed below are shown as solid blue and red paths in figure 7A, and their
412 corresponding model age-eU curves (Fig. 7B) are indicative of the range of age-eU
413 curves that result from our refined scenarios. These specific temperatures for the lower
414 elevation sample group include: 200 °C for the Proterozoic intermediate and 160 °C for
415 the Phanerozoic maximum, and, for the higher elevation group, 170 °C for the
416 Proterozoic intermediate and 130 °C for the Phanerozoic maximum.
417 Both sample group thermal histories consist of initial cooling from 1800-1600 Ma
418 followed by a second stage of cooling beginning at either 900 or 700 Ma with a wide
419 range of potential intermediate temperatures (shown as the red and blue dashed-line *t-T*
420 segments between 1800 and 525 Ma in Fig. 7A). This range of Proterozoic intermediate
421 temperatures extends from 135 to 220 °C for the lower elevation samples (transparent red
422 *t-T* segments) and from 140 to 220 °C for the higher elevation samples (transparent blue
423 *t-T* segments). These temperature ranges yield age-eU results similar to those shown in
424 figure 7B for a given sample group, provided that the same maximum Phanerozoic
425 temperatures are used as described below. Model age-eU curves are also similar for the
426 second cooling stage at either 900 or 700 Ma and it is difficult to distinguish between the
427 two options for Neoproterozoic cooling. Importantly though, paths with two-stage
428 cooling from 1800-1600 Ma and 1300-1000 Ma capture fewer ages than the two-stage
429 900 or 700 Ma paths at any given combination of tested temperatures. The 1800-1600
430 Ma, 1300-1000 Ma paths yield a narrower range of model ages at low burial
431 temperatures, which reproduce fewer of the observed ages from the high elevation
432 sample group.

433 The range of subsequent maximum Phanerozoic burial temperatures are 155 to
434 160 °C for the lower elevation group of samples, and 120 to 140 °C for the higher
435 elevation group (shaded red and blue *t-T* segments between 525 and 0 Ma in Fig. 7A).
436 Again, temperatures in either of these ranges yield age-eU curves similar to those in
437 figure 7B when paired with their counterpart intermediate Proterozoic temperatures listed
438 above. A minimum 15 °C difference between the two sample groups is therefore required
439 just prior to Laramide cooling. If the offset between these two *t-T* paths is at least 15 °C
440 during the Laramide, then the offset should be roughly the same throughout both thermal
441 histories, which reduces the lower-bound of potential intermediate Proterozoic
442 temperatures for the higher elevation samples from 220 to 205 °C, and the upper-bound
443 for the lower elevation samples from 135 °C to 155 °C. In figure 7A, this tighter region
444 of *t-T* space is shown by the transparent red and blue shading between 1800 and 525 Ma.
445 As a further condition of the 15 °C offset, the lower elevation samples were also likely at
446 higher temperatures during deposition of the middle Cambrian Flathead Sandstone than
447 the higher elevation samples, which is reflected in the *t-T* paths in figure 7A.
448 The observations from figure 7, combined with the results from our representative
449 *t-T* path tests, suggests that the Wind River age-eU correlations are less sensitive to
450 precise intermediate Proterozoic temperatures, but the overall shape of the path (single
451 versus two-stage Precambrian cooling paths) and the timing of cooling are required. The
452 maximum burial temperatures achieved prior to Laramide cooling are also important, as
453 figure 7 demonstrates, with a 15-40 °C difference between the higher and lower elevation
454 sample groups giving markedly different age-eU curves. Only ~600 m of topographic
455 elevation separates the lowest low elevation sample (WY-98-89) from the highest high

456 elevation sample (WY-90-89), and so a 15-40 °C difference might seem too high, even if
457 we consider a relatively cold geothermal gradient (15 °C/km). However, we note that
458 Paleozoic strata dip ~10-15° on the northeast side of the Wind River, and if these rocks
459 are restored to horizontal, combined with ~15 km of lateral distance between samples
460 WY-98-89 and WY-90-89, then there is approximately 3 to 4.5 km of stratigraphic
461 separation relative to a Great Unconformity paleosurface.
462
463 **6. Discussion**
464 Given the lack of Proterozoic *t-T* constraints from the region, our results provide
465 the first robust thermochronologic constraints on the thermal history of the Archean cores
466 of these Laramide ranges. Our thermal modeling yields a best-fit *t-T* history for Bighorn
467 Mountains consisting of two stages of Proterozoic cooling (1800-1600 Ma and 900-525
468 Ma), followed by reburial to 110-115 °C just prior to a final phase of "Laramide" cooling
469 between 85-60 Ma (Fig. 6). The histories that best agree with the observed ages for the
470 Wind Rivers consist of the same two stages of Proterozoic cooling as the Bighorn data,
471 with Phanerozoic burial of the structurally deepest samples (WY-98-89 and WY-96-89)
472 to a maximum temperature of 155-160 °C and the remaining samples buried to 120-140
473 °C prior to all samples experiencing "Laramide" cooling between 60-40 Ma to 50 °C.
474 The maximum Phanerozoic burial temperatures in the Wind River Range therefore
475 exceeded those of the Bighorn Mountains. The best-fit *t-T* constraints for both ranges do
476 not capture several of the youngest ages at high (>1000 ppm) eU values. In addition, the
477 eU concentrations for these zircons suggest that they should be metamict and possess
478 zero ages. Because the observed ages are not zero, this suggests that some zone of

crystallinity remains in these highly damaged grains that ZRDAAM is currently unable to account for. Nevertheless, we emphasize that our best-fit paths capture the dominate trend of the data, supporting our interpretation that radiation damage is the primary control on age variability.

Major cooling events in the best-fit thermal histories for both datasets coincide with major tectonic events that affected Laurentia during the Paleoproterozoic-Mesozoic (Fig. 2). Initiation of cooling ca. 1800-1600 Ma in both ranges coincides with Yavapai-Mazatzal tectonic activity (~ 1760-1600 Ma) (Whitmeyer and Karlstrom, 2007). Evidence for cratonic cooling during orogenesis is found to the south of our study region along the Laramie Peak shear zone (Chamberlain, 1998), but our thermochronologic data is the first evidence that the interior of the Wyoming craton also experienced cooling during this time. The Neoproterozoic cooling event required by these data also coincides with documented rifting in the midcontinent, the Rocky Mountains, the southern limit of the Wyoming craton, and the west-central U.S. (Utah, Idaho, Nevada) (van Schmus, 1992; Marshak and Paulsen, 1996; Timmons et al. 2001; Yonkee et al., 2014). Our results suggest that this cooling may have extended much farther into the craton than previously documented.

Although our thermal modeling is an overall good fit to the geologic record in western Laurentia, slight differences exist between the Bighorn and Wind River samples that allow us to make more detailed interpretations. We highlight two important differences between the Bighorn and Wind River age-eU correlations: 1) the Bighorns' continuously negative age-eU correlation begins at ~960 Ma (much older than the oldest Wind River age of 582 Ma), and 2) the Bighorn’s age-eU correlation has a young cluster

of ages (~30-7 Ma) at ~1500 eU instead of an age-eU pediment. Negative age-eU correlations require that the highest eU and therefore most damaged grains have higher diffusivities than their lower eU counterparts. The transition from low to high diffusivity occurs when grains have accumulated an alpha dose in excess of ~5×10^{17} α/g, and if all grains in a sample compose a single negative correlation, then all grains have at least more accumulated damage than ~5×10^{17} α/g (Guenthner et al. 2013). Importantly, the oldest age in a negative age-eU correlation represents the *minimum* amount of time over which this damage accumulation must have occurred. If the annealing kinetics of the damage that affects He diffusion are the same as those for fission tracks, then all of the grains in the Bighorn dataset have been cooler than ~220 °C (lower temperature bound for the ZFT PAZ) since at least ~950 Ma.

The cluster of young ages at ~1500 ppm eU in the Bighorn dataset contrasts with the age-eU tail at similar eU concentrations in the Wind River dataset. Guenthner et al. (2014) showed that age-invariant samples across a wide range of eU require relatively rapid cooling through the wide range of T_c's associated with the wide range of accumulated damage. The ages of the tail correspond to the timing of this cooling event, which for the Wind Rivers, is at ~ 60 Ma. In contrast, the Bighorn's age-eU correlation shows no age-eU tail, and instead is continuously negative from old (957 Ma) to young (7 Ma) ages. In our best-fit model *t-T* paths (Fig. 7), the Wind River dataset cools from between 160-125 °C to 50 °C between 60 and 40 Ma, whereas the Bighorn dataset cools from 115-110 to 50 °C between 85 and 60 Ma. Because the Wind Rivers experienced higher Phanerozoic burial temperatures, and cooling from higher to lower temperatures over a shorter time period than the Bighorns, a wider range of eU grains were fully reset

525 and that same wide range of grains “closed” at roughly the same time to yield the same
526 ages and form a tail.
527 Differences in the outcrop position of the samples with respect to the Great
528 Unconformity suggest that contrasting structural depths within Archean basement could
529 explain the different maximum burial temperatures in the *t-T* histories from each range.
530 The majority of samples from the Bighorn Mountains are from locations relatively close
531 to the outcrop exposure of the Archean-Cambrian unconformity, whereas the samples
532 from the Wind River Range were collected from locations likely significantly below this
533 structural depth. We speculate that the Bighorn samples were located closer to the paleo-
534 surface than the Wind River Range samples prior to the onset of Cambrian passive
535 margin sedimentation. Differences in the structural depth of samples across the Wind
536 River Range transect yield two distinct thermal histories. In contrast, samples from the
537 Bighorn Mountains yield one best-fit thermal history, likely because the structural relief
538 across the sample transect is significantly less than that in the Wind River Range. The
539 characteristics of each range’s age-eU correlation therefore serve as examples of how
540 contrasting thermal histories can produce different and decipherable age-eU correlations.
541 This dataset of variable, but systematically correlated, zircon He ages provides
542 additional information that lower temperature thermochronometers (apatite He and AFT)
543 cannot resolve. Recognition of the effects of radiation damage on He diffusivity allow for
544 thermal modeling of samples which show large variation in single grain ages, while not
545 excluding any replicates. Using the distribution of ages correlated with eU, the modeling
546 here shows evidence for previously unrecognized cooling events within the Wyoming
547 craton and constraints on previously documented burial heating events in the Proterozoic

and Phanerozoic, respectively. The addition of significantly older parts of the region's thermal history to existing models on the most recent exhumation event furthers our understanding of the thermal history of Laurentian basement in the northern Rocky Mountain region and poses potential for understanding ancient tectonic and thermal histories in other regions of exposed basement terranes.

Acknowledgements: We thank James R. Steidtmann at the University of Wyoming for providing the separates from his seminal work in the Wind River Range to Barbara Carrapa. We thank Barbara Carrapa for use of these separates and scientific input on this manuscript. We thank Uttam Chowdhury for analytical support. We acknowledge support from ExxonMobil to W.R. Guenthner, EAR-0910577 to P.W. Reiners and ChevronTexaco Fellowships awarded to D.A. Orme and A.K. Laskowski.

Appendix I: Zircon (U/Th)/He Data Table
Appendix II: Thermal history model input table

Supplementary Material:
Figure 1: age-elevation plot of Wind River Range and Bighorn dataset

References

Ault, A.K., Flowers, R.M., and Bowring, S.A., 2013. Phanerozoic surface history of the Slave craton. Tectonics, 32, 1066-1083.

Ault, A.K., Flowers, R.M., and Bowring, S.A., 2009. Phanerozoic burial and unroofing of the western Slave craton and Wopmay orogen from apatite (U-Th)/He thermochronometry. Earth and Planetary Science Letters, 284, 1-11.

Cerveny, P. F., and Steidtmann, J. R., 1993. Fission track thermochronology of the Wind River Range, Wyoming: evidence for timing and magnitude of Laramide exhumation. Tectonics, 121. 77–91.

Chamberlain, K.R., 1998, Medicine Bow orogeny: Timing of deformation and model of crustal structure produced during continent-arc collision, ca.1.78Ga, south-eastern Wyoming: Rocky Mountain. Geology 33, 259–277.

Chamberlain, K.R., Frost, C.D., and Frost, B.R., 2003. Early Archean to Mesoproterozoic evolution of the Wyoming Province: Archean origins to modern lithospheric architecture. Canadian Journal of Earth Science 40, 1357-1374.

585 Crowley, P. D., Reiners, P. W., Reuter, J.M, and Kaye, G. D., 2002. Laramide
586 exhumation of the Bighorn Mountains, Wyoming: an apatite (U-Th)/He
587 thermochronology study. Geology 301, 27–30.

588 Fan, M., and Carrapa, B. 2014. Late Cretaceous–early Eocene Laramide uplift,
589 exhumation, and basin subsidence in Wyoming: Crustal responses to flat slab
590 subduction. Tectonics 33, 508–529.

591 Flowers, R.M., Ketcham, R.A., Shuster, D.L., Farley, K.A., 2009. Apatite (U-Th)/He
592 thermochronometry using radiation damage accumulation and annealing model.
593 Geochim. Cosmochim. Acta 73, 2347-2365.

594 Frost, C.D, and Frost, B.R., 1993. The Archean history of the Wyoming province *in*
595 Geology of Wyoming, eds. Snoke, A.W., Steidtmann, J.R., and Roberts, S.M.:
596 Geological Survey of Wyoming Memoir 5, 58-78.

597 Gautheron, C., Barbarand, J., Ketcham, R. A., Tassan-Got, L., Van Der Beek, P., Pagel,
598 M., et al. 2013). Chemical influence on α-recoil damage annealing in apatite:
599 Implications for U–Th)/He dating. Chemical Geology 351C, 257–267.

600 Gleadow, A. J. W., Kohn, B. P., Brown, R. W., O'Sullivan, P. B., and Raza, A., 2002.
601 Fission track thermotectonic imaging of the Australian continent. Tectonophysics,
602 349, 5–21.

603 Guenthner, W.R., Reiners, P.W., Tian, Y., 2014. Interpreting date-eU correlations in
604 zircon (U-Th)/He datasets: A case study form the Longmen Shan, China. Earth and
605 Planetary Science Letters, 403, 328-339.

606 Guenthner, W.R., Reiners, P.W., DeCelles, P.G., and Kendall, J., 2015. Sevier-belt
607 exhumation in central Utah constrained from complex zircon (U-Th)/He datasets:
608 Radiation damage and He inheritance effects on partially reset detrital zircons. Geol.
609 Soc. Am. Bull. 127:323.
610
611 Guenthner, W.R., Reiners, P.W., Ketcham, R.A., Nasdala, L., and Giester, G., 2013.
612 Helium diffusion in natural zircon: Radiation damage anisotropy, and the
613 interpretation of zircon (U-Th)/He thermochronology. American Journal of Science,
614 313, 145-198.

615 Heimlich, R. A., and Armstrong, R. L. 1972. Variance of Precambrian K-Ar biotite dates,
616 Bighorn Mountains, Wyoming. Earth and Planetary Science Letters, 141. 75–78.

617 Hoffman, P. F. 1988. United plates of America, the birth of a craton: Early Proterozoic
618 assembly and growth of Laurentia. Annu. Rev. Earth Planet. Sci. 16, 543–603.

619 Houston, R.S., 1993, Late Archean and Early Proterozoic geology of the Wyoming
620 province, *in* Snoke, A.W., et al., eds., Geology of Wyoming. Geological Survey of
621 Wyoming Memoir 5, 78–116.

Ketcham, R. A., 2005. Forward and Inverse Modeling of Low-Temperature Thermochronometry Data. Reviews in Mineralogy and Geochemistry 58, 275–314.

Kohn, B. P., Gleadow, A. J. W., Brown, R. W., Gallagher, K., Lorencak, M., and Noble, W.R., 2005. Visualizing thermotectonic and denudation histories using apatite fission track thermochronology. Rev. Mineral. Geochem. 58, 527–565.

Marshak, S., and Paulsen, T., 1996. Midcontinent U.S. fault and fold zones: A legacy of Proterozoic intracratonic extensional tectonism. Geology 24, 151–154.

Marshak, S., Karlstrom, K., Timmons, J.M., 2000. Inversion of Proterozoic extensional faults: An explanation for the pattern of Laramide and Ancestral Rockies intracratonic deformation, United States. Geology 278, 735-738.

Mitra, G. and Frost, B.R., 1981. Mechanisms of deformation within Laramide and Precambrian deformation zones in basement rocks of the Wind River Mountains. University of Wyoming Contributions to Geology 19, 161-173.

Mueller, P.A. and Frost, C.D., 2006. The Wyoming Province: a distinctive Archean craton in Laurentian North America. Canadian Journal of Earth Science 43, 1391-1397.

Patel, S.C., Frost, C.D., and Frost, B.R., 1999. Contrasting responses of Rb-Sr systematics to regional and contact metamorphism, Laramie Mountains, Wyoming, USA. J. Metamorphic Geol., 17, 259-269.

Peterman, Z.E. and Hildreth, R.A., 1978. Reconnaissance geology and geochronology of the Precambrian of the Granite Mountains, Wyoming. U.S. Geological Survey, Professional Paper 1055 p.

Peterman, Z.E., 1979. Geochronology and the Archean of the United States. Economic Geology 74, 1544-1562.

Peyton, S. L., Reiners, P. W., Carrapa, B., and DeCelles, P.G., 2012. Low-temperature thermochronology of the northern Rocky Mountains, western U.S.A. American Journal of Science 312, 145–212.

Peyton, L. and Carrapa, B., 2013. An overview of low-temperature thermochronology in the Rocky Mountains and its applications to petroleum system analysis, in C. Knight and J. Cuzella, eds., Application of structural methods to Rocky Mountain hydrocarbon exploration and development. AAPG Studies in Geology, 37-70.

Powell, J., Schneider, D., Stockli, D, and Fallas, K. 2016) Zircon (U-Th)/He thermochronology of Neoproterozoic strata from the Mackenzie Mountains, Canada: Implications for the Phanerozoic exhumation and deformation history of the north Canadian Cordillera. Tectonics 35, doi: 10.1002/2015TC003989.

Reiners, P. W., Spell, T. L., Nicolescu, S., and Zanetti, K. A., 2004. Zircon (U-Th)/He thermochronometry: He diffusion and comparisons with $^{40}Ar/^{39}Ar$ dating. Geochimica et Cosmochimica Acta 68, 8, 1857–1887.

Reiners, P. W., and Farley, K. A. 2001. Influence of crystal size on apatite (U-Th)/He thermochronology: an example from the Bighorn Mountains, Wyoming. Earth and Planetary Science Letters 188, 413– 420.

Schruben, P. G., R. E. Arndt, and W. J. Bawiec 1997. Geology of the Conterminous United States at 1:2,500,000 Scale—A Digital Representation of the 1974 P.B. King and H.M. Beikman Map. U.S. Geological Survey Digital Data Series DDS-11, Release 2.

Steidtmann, J.R., L.T. Middleton, and M.W. Shuster, 1989. Post-Laramide Oligocene uplift in the Wind River Range, Wyoming. Geology, 17, 38-41.

Stevens, A., Balgord, E.A., and Carrapa, B., 2016. Revised exhumation history of the Wind River Range, WY, and implications for Laramide tectonics. Tectonics 35, doi:10.1002/2016TC004126.

Timmons, J.M., Karlstrom, K.E., Dehler, C.M., Geissman, J.W., and Heizler, M.T., 2001. Proterozoic multistage ca. 1.1 and ca. 0.8 Ga extension in the Grand Canyon Supergroup and establishment of northwest and north-trending tectonic grains in the southwestern United States. Geol. Soc. Am. Bull., 1132. 163-181.

Van Schmus, W.R., 1992, Tectonic setting of the midcontinent rift system: Tectonophysics 15, pp. 712.

Whitmeyer, S.J., Karlstrom, K.E., 2007. Tectonic model for the Proterozoic growth of North America. Geosphere 3, 220–259.

Yonkee, W.A., Dehler, C.D., Link, P.K., Balgord, E.A., Keeley, J.A., Hayes, D.S., Wells, M.L., Fanning, C.M., and Johnston, S.M., 2014, Tectono-stratigraphic framework of Neoproterozoic to Cambrian strata, west-central U.S.: Protracted rifting, glaciation, and evolution of the North American Cordilleran margin. Earth Science Reviews 136, 59–95.

Figure Captions

Figure 1: Geologic sketch map of the Wind River Range, Bighorn Mountains and surrounding areas showing Zircon (U-Th)/He sample localities. The base map is a shaded, colored ASTER digital elevation model created using GeoMapApp (geomapapp.org). Map unit pCg demarcates the aerial extent of Precambrian crystalline basement rocks. Geology adapted from Schruben et al., (1997). Inset tectonic map adapted from Peyton and Carrapa (2013).

Figure 2: Major tectonic events affecting the Archean Wyoming Province from ca. 3.0 Ga to the present. Black vertical boxes denote thermochronologic constraints currently available for Archean basement. Constraints from Hoffman (1988), Chamberlain et al. (2003), Peterman and Hildreth (1978), and Peyton et al. (2012).

Figure 3: Zircon (U-Th)/He age-effective Uranium (eU) correlations for the (A) Wind River Range (54 ages) and (B) Bighorn mountains (32 ages). Samples BH12 and BH17 include data from Guenthner et al. (2013).

Figure 4: (A) End-member *t-T* histories tested for the Wind River Range (red) and Bighorn Mountains (blue). Scenario 1 rapidly cools from 350 to 20 °C between 2600-2500 Ma, reflecting cooling from high-grade metamorphism associated with the Trans-Hudson orogeny. In Scenario 2, cooling initiates between 700-525 Ma, reflecting the formation of the Great Unconformity. Phanerozoic thermal histories are held constant. (B) Resulting envelopes which show how well the combined effects of grain size and radiation damage capture the observed ages Modeled grain sizes for the Wind River and Bighorn datasets average 75 ± 39 μm and 57 ± 26 μm, respectively. The output consists of a central curve (mean grain size) encompassed by a shaded envelop (±2 grain size standard deviations).

Figure 5: (A) Representative *t-T* paths testing rapid cooling associated with four Proterozoic tectonic events between 1800-900 Ma as discussed in the text. (B) Model output for thermal histories and observed data for the Bighorn and Wind River datasets. Numbered *t-T* paths in panel insets correspond to the *t-T* paths shown in Part A. For the Bighorns, none of the modeled curves are a good fit to the observed data. For the Wind Rivers, scenarios 2 (inset iv) and 3 (inset vi) capture 77% of the observed dataset, but both fail to capture young ages at low eU values.

Figure 6: (A) Representative *t-T* paths testing two-stage monotonic cooling with prolonged residence at intermediate temperatures. (B) Scenario 2 (inset iii), rapid cooling at 1800-1600 Ma and 900-525 Ma, best captures the negative age-eU trend of the dataset. Scenarios 1-3 yield roughly the same fits to the Wind Rivers dataset and fail to capture ages at eU values greater than ~300 ppm.

Figure 7: Refined, best-fit *t-T* solutions for the Bighorn Mountains. (A) Scenario 1 has a Proterozoic temperature of 160 °C and Mesozoic burial to 115 °C. Scenario 2 cools to 155 °C in the Proterozoic and 110 °C in the Mesozoic. (B) Best-fit envelopes for the *t-T* paths of Part A.

735 **Figure 8:** Refined, best-fit *t-T* solutions for the Wind River Range. (A) *t-T* paths with a
736 range of Proterozoic intermediate temperatures extending from 135-220 °C for low-
737 elevation samples (red envelope) and from 140-220 °C for higher elevation samples (blue
738 envelope). Maximum Phanerozoic burial temperatures are 155 to 160 °C for the lower
739 elevation group of samples, and 120 to 140 °C for the higher elevation group. (B) Best-fit
740 envelopes for low-elevation (red) and high-elevation (blue) samples which best captures
741 the data and the long-tail at high eU values.

742

Figure 1

Click here to download Figure: figure 1 Geologic Setting copy.pdf

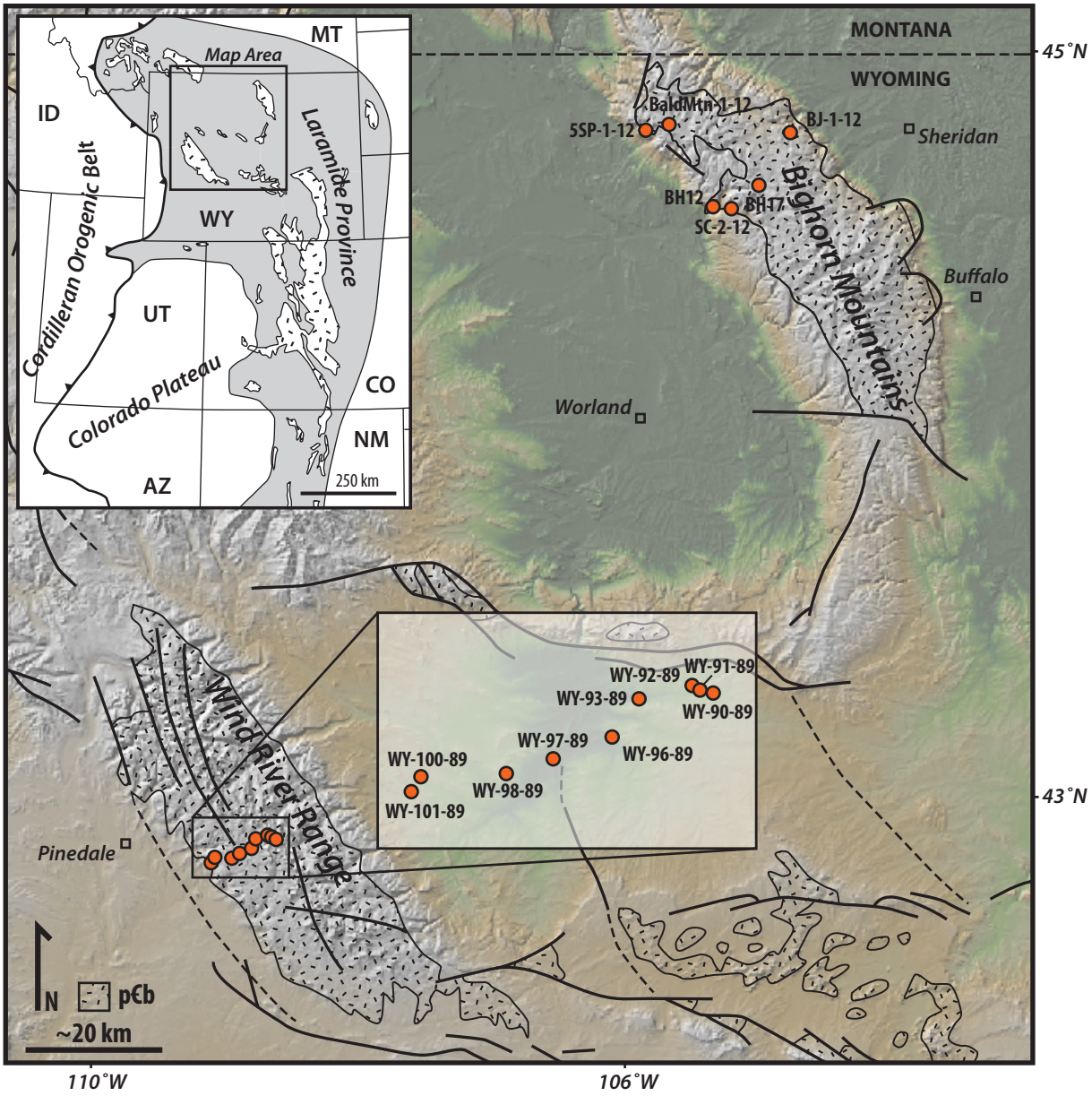

Figure 2 Tectonic History and Constraints on Forward Models

Click here to download Figure: figure 2 Geologic Con

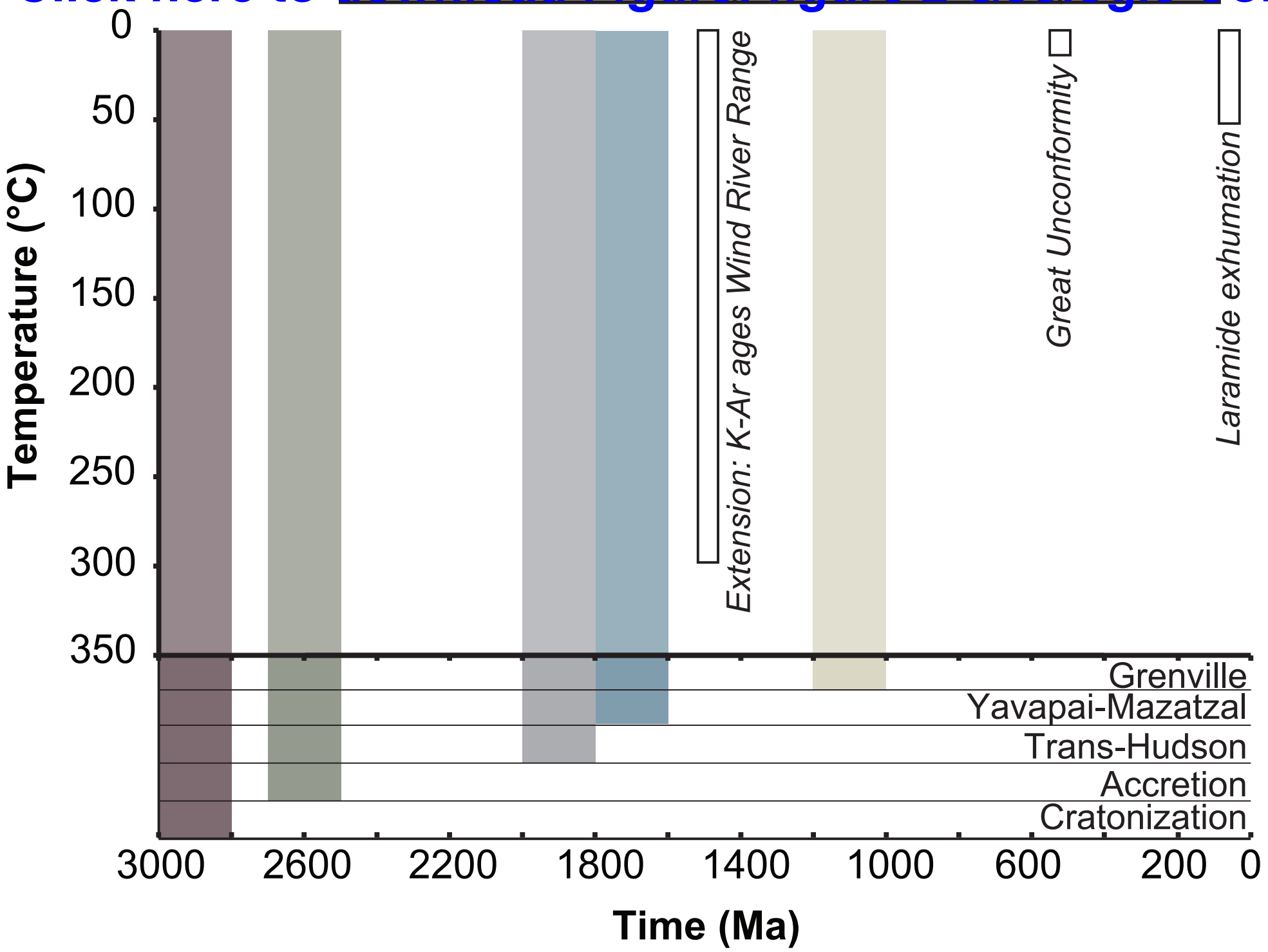

Figure 3

Click here to download Figure: figure 3 Laramides.pdf

A. Wind River Range

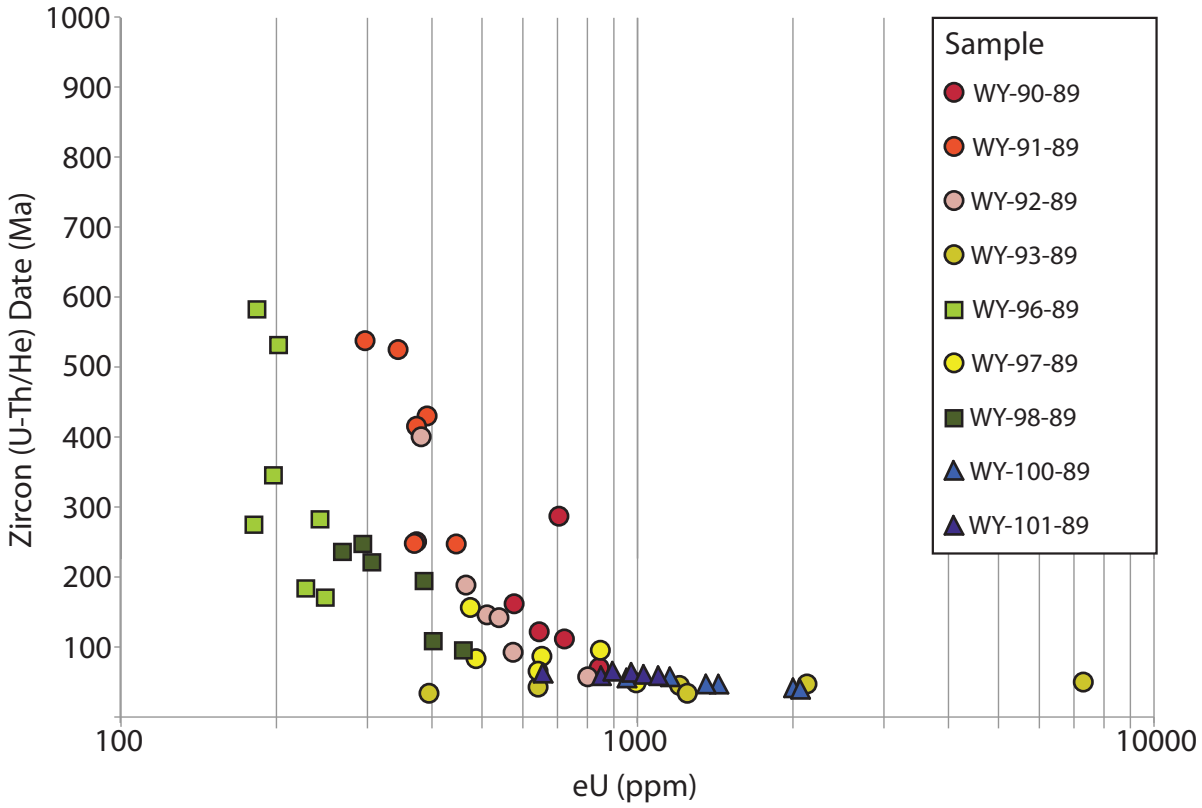

B. Bighorn Mountains

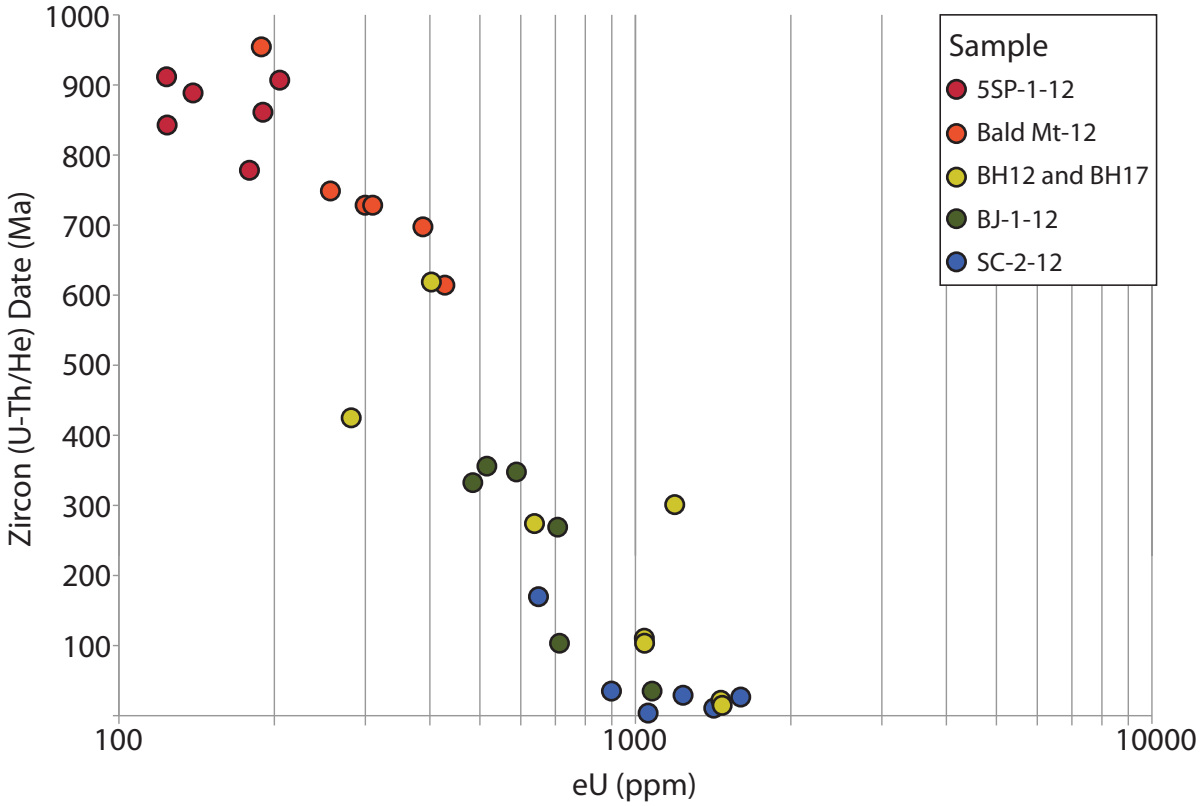

Figure 2:

Figure 4

Click here to download Figure: figure 4 endmember results no inset.pdf

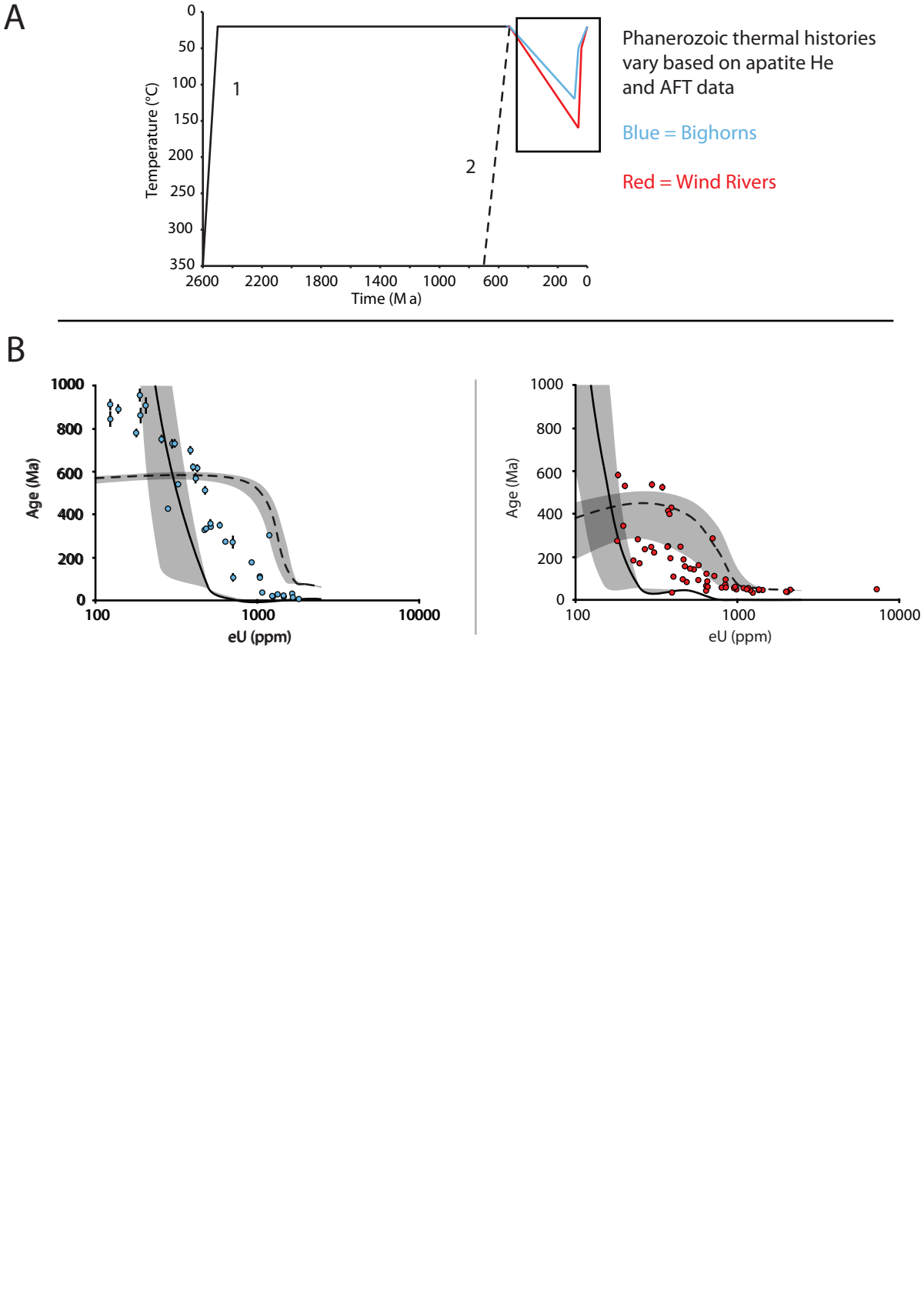

Figure 5

Click here to download Figure: figure 5 representative rapid.pdf

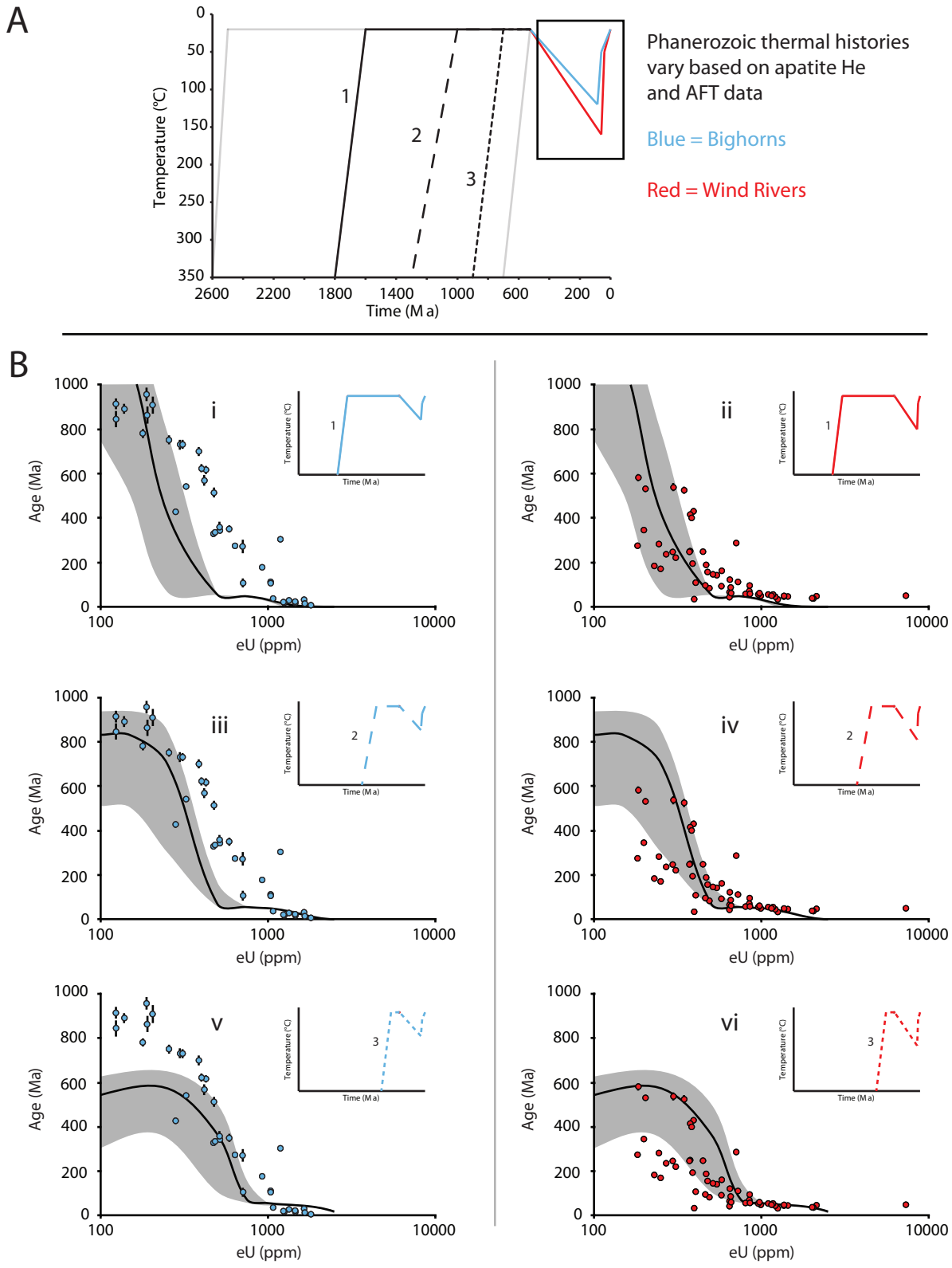

Figure 6

Click here to download Figure: figure 6 representative 2 stage.pdf

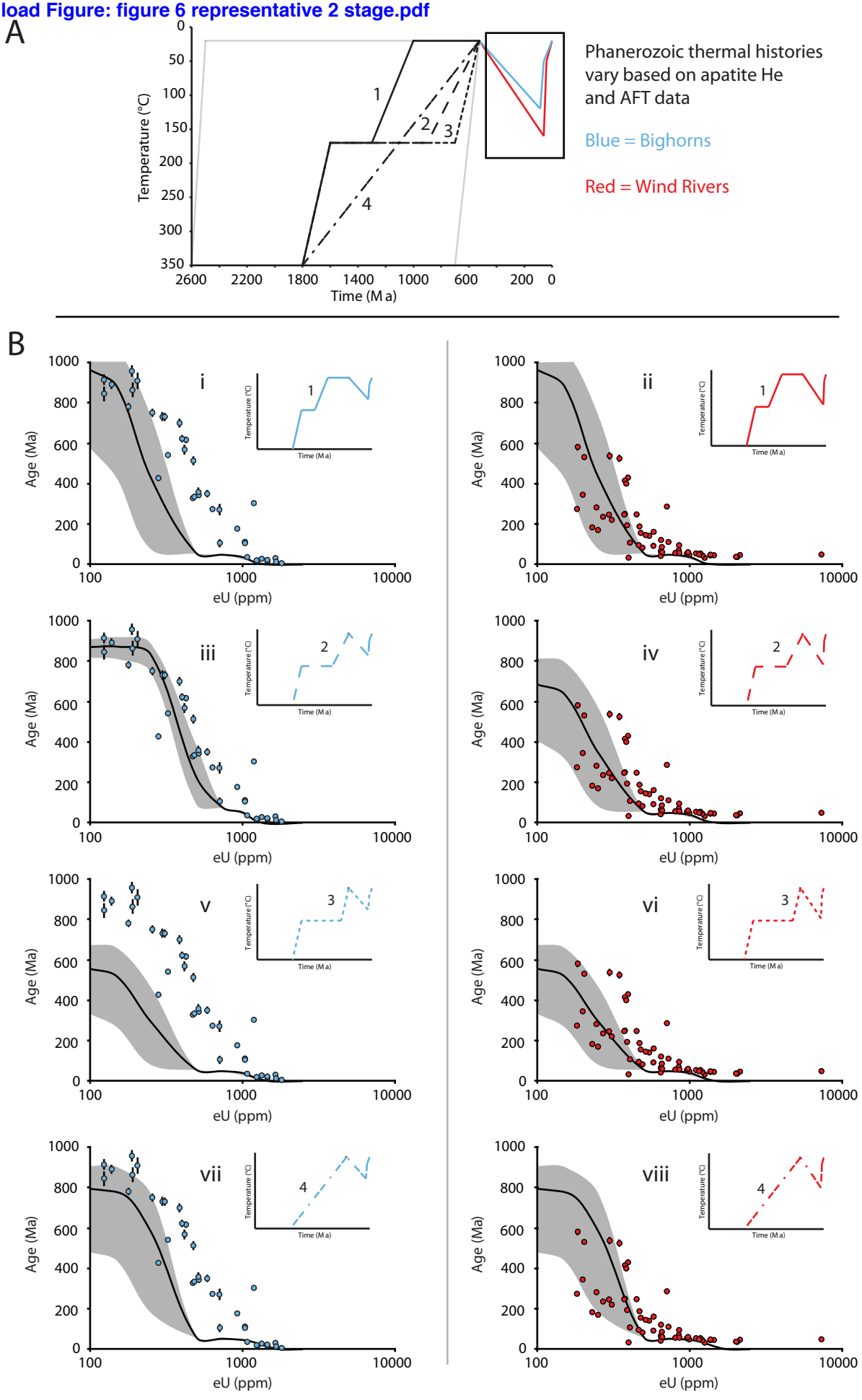

Figure 7

Click here to download Figure: figure 7 Bighorns best solution.pdf

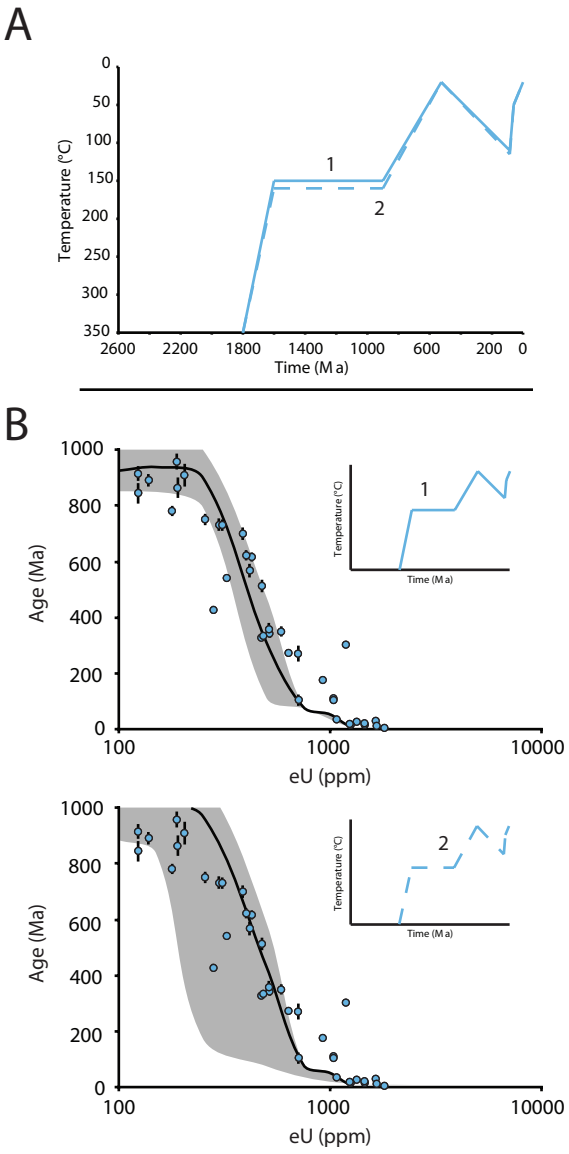

Figure 8

Click here to download Figure: figure 8 Wind Rivers best solution_updated.pdf

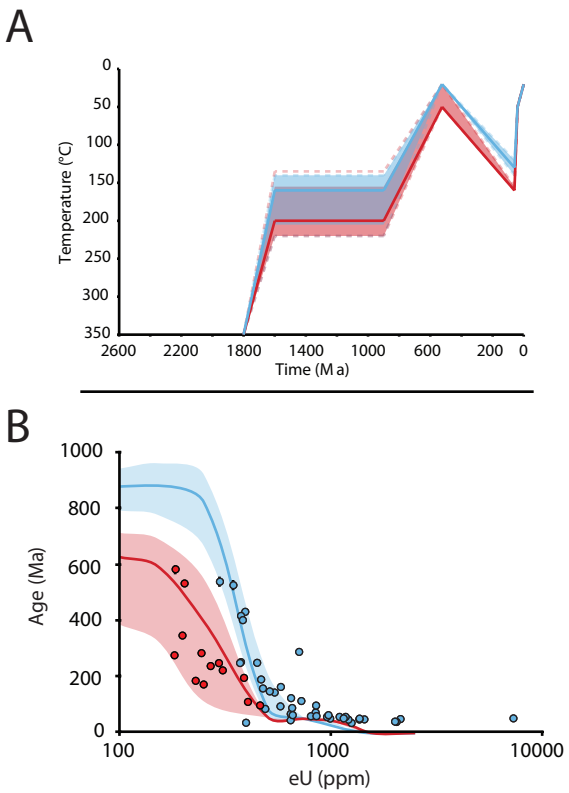

Supplementary material: age-elevation plot

Click here to download Supplementary material for online publication only: Supplementary- Figure 1.pdf

Supplementary material: Zircon (U-Th)/He results

Click here to download Supplementary material for online publication only: Appendix I- All Zircon Helium Data.pdf

Supplementary material for review only (e.g., accepted "in press" reference files)

Click here to download Supplementary material for review only (e.g., accepted "in press" reference files): Appendix II.pdf